

Methodology development and validation of integrating sphere measurement of small size tissue specimens

Yijing Xie¹, Eli Nabavi^{1,2}, Jonathan Shapey^{1,3}, Micheal Ebner¹, and Tom Vercauteren¹

¹ School of Biomedical Engineering & Imaging Sciences, King's College London, London SE1 7EH, UK

² CMR Surgical Ltd, Cambridge CB24 9NG, UK

³ Department for Neurosurgery, King's College Hospital, London UK

E-mail: yijing.xie@kcl.ac.uk

Abstract. Optical imaging modalities are non-ionizing methods with significant potential for noninvasive, portable, and cost-effective medical diagnostics and treatments. The design of critical parameters of an optical imaging system depends on a thorough understanding of optical properties of the biological tissue within the purposed application. Integrating sphere technique combined with inverse adding doubling algorithm has been widely used for determination of biological tissue *ex vivo*. It has been studied for tissues typically with a large sample size (approx. 20 x 20 mm) and over a spectral range of 400 nm to 1100 nm. The aim of this study is to develop a methodology for calculating optical absorption μ_a and reduced scattering μ'_s of small size (approx. 6 x 8 mm) biological tissues from reflectance and transmittance measurements at a wide spectral range of 400 to 1800 nm. We developed a small sample adaptor kit to allow integrating sphere measurements of samples with small sizes using a commercial device. Dual beam single integrating sphere technique was used to the total transmittance (T_{total}) and total reflectance (R_{total}) measurements of samples, and inverse adding doubling (IAD) was used to convert the measurements T_{total} and R_{total} to optical properties. We proposed a two-tier IAD algorithm to mitigate the profound cross-talk effect in reduced scattering using IAD. We evaluated the two-tier IAD with both simulated data by Monte Carlo Simulation and data obtained from phantom experiments. We also investigated the accuracy the proposed work flow of using small sample kit and condensed incident light beam. We found that the small sample measurements despite with condense beam size led to overestimated absorption coefficient across the whole wavelength range while the spectrum shape well preserved. Our proposed method of a two-tier IAD and small sample kit could be a useful and reliable tool to characterise optical properties of biological tissue *ex vivo* particularly when only small size samples are available.

Keywords: integrating sphere, inverse adding doubling, tissue optical properties, hyperspectral imaging, Monte-Carlo simulation

1. Introduction

Optical imaging modalities have become valuable tools in clinical applications, providing real-time tissue structural, molecular and functional information for diagnosis, or guiding surgical or therapeutic interventions [1, 2, 3, 4, 5, 6, 7, 8, 9, 10, 11, 12, 13, 14, 15]. The design and development of optical imaging rely on a thorough understanding of the optical properties of tissue typically characterized by the absorption and reduced scattering coefficients, μ_a and μ'_s , respectively. Inverse adding doubling (IAD) with integrating sphere measurements is one of the most widely used method to derive optical properties of *ex vivo* tissue samples. The open source IAD algorithm can be conveniently used with integrating sphere measurements where the geometrical parameters such as port size of an integrating sphere, number of measurements, dimensions of the sphere, size of the incident light beam and the refractive index of the given biological sample have been considered and accounted in the algorithm [16]. Most tissue optics research has employed light in the visible and near-infrared regions of the spectrum (VIS-NIR 400 nm - 1100 nm), to characterise the perfusion status of a tissue by measuring the concentration of oxygenated and deoxygenated hemoglobin of which the primary absorption peaks are in the visible range [17, 18]. In addition, some studies focus on the tissue water and lipid concentrations by using signals detected at the long wavelength of 900 to 1000 nm [19, 20]. Further more, the tissue samples studied were either in large size as their naive form that were able to cover a standard sphere port or patched together [21]. The purpose of this study was to develop a methodology for calculating optical absorption (μ_a) and reduced scattering (μ'_s) of small size (approx. 6 x 8 mm) biological tissues from reflectance and transmittance measurements at a wide spectral range of 400 to 1800 nm. We developed a small sample kit to allow integrating sphere measurements of samples with small sizes using a commercial spectrophotometer. A dual beam single integrating sphere technique was used to the total transmittance (T_{total}) and total reflectance (R_{total}) measurements of samples, and inverse adding doubling (IAD) was used to convert the measurements T_{total} and R_{total} to optical properties. We proposed a two-tier IAD algorithm to mitigate the profound cross-talk effect in reduced scattering using IAD. We evaluated the two-tier IAD with both simulated data by Monte Carlo Simulation and data obtained from phantom experiments. We also investigated the accuracy the proposed work flow of using small sample kit and condensed incident light beam.

2. Materials & Methods

2.1. Integrating sphere measurement

In this study, we used a commercial dual beam high performance spectrophotometer system (Lambda 750s, Perkin Elmer) equipped with a 100 mm single integrating sphere module (L6020371, Perkin Elmer) for transmittance and reflectance measurements. The system is supplied with a photomultiplier tube detector (PMT, 250 - 860 nm)

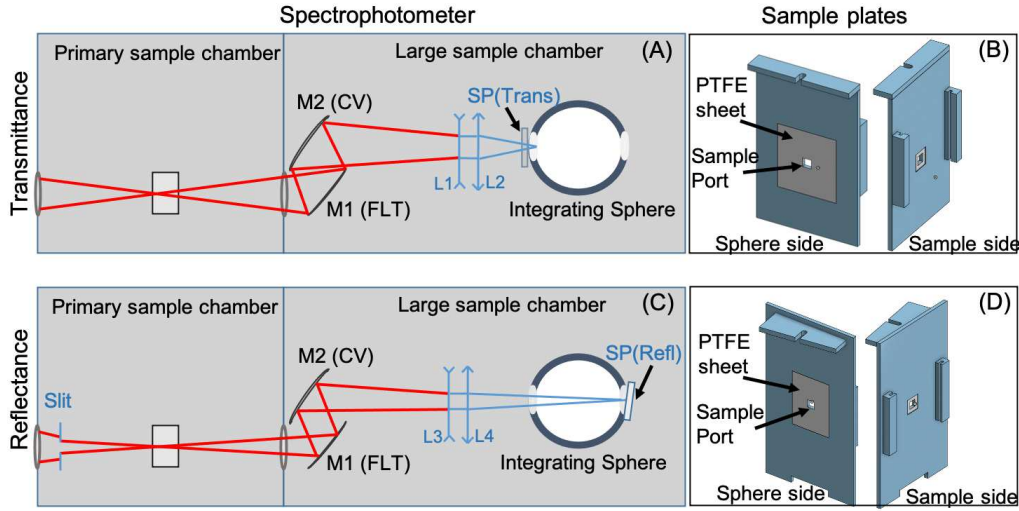


Figure 1. The small sample kit includes lens assembly and sample plate for adjusting sample aperture size and holding sample slide. Adaptation of spectrophotometer: a) adjustable slit; b) normal transmittance setup, c) adapted transmittance setup with lens and port adapter, d) normal reflectance setup, e) adapted reflectance setup with port adapter (lens not shown [in similar location to (c)])

and a Indium gallium arsenide detector (InGaAs, 860 nm - 2500 nm), covering a wide wavelength range from 200 to 2500 nm. The system's performance in terms of wavelength calibration and measurement accuracy has been validated by the manufacturer. It has been used in research and industrial labs as a standard tool for precise analysis of materials in various applications [22, 23, 24]. A schematic illustration of the original spectrophotometer setup and the modified set up with small sample kits presenting is shown in Figure 1 (A, C). The original sample port size at transmittance port is 11 mm (w) x 24 mm (h), and the reflectance port is 17 mm (w) x 22 mm (h); the incident light beam size is measured around 3 mm (w) x 15 mm (h) at the transmittance port, and 6.5 mm (w) x 13.5 mm (h) at the reflectance port. The basic operation principle of performing reflectance and transmittance measurements using spectrophotometer with an integrating sphere, respectively, are also sketched in Figure 1(A, C). All measurements were carried out relative to a diffuse optical standard, Spectralon® (SRS-99-020, Labsphere), which is a white Lambertian material with diffuse reflectance values between 95–99% in the wavelength region from 250 nm to 2500 nm. With the aforementioned integrating sphere configuration, total transmittance and total reflectance are measured at all experiments conducted in this study and are denoted as T_{total} and R_{total} , respectively, except otherwise stated.

2.2. Small sample kit

The original setup of the spectrophotometer can be used to obtain measurement of various solid materials of which the size satisfy the constrain that is the distance (h)

Table 1. Small sample kit parameters

Reduced port size	Measurement type	Lenses	Slit width	Beam size at the port
3 mm	Transmittance	L1 -150, L2 60	5 mm	1 x 1.5 mm
3 mm	Reflectance	L3 -150, L4 200	3 mm	2 x 2 mm
5 mm	Transmittance	L1 -150, L2 60	no slit	2 x 2 mm
5 mm	Reflectance	L3 -150, L4 200	5 mm	2 x 3.5 mm

L1: LC1611 Thorlabs; L2: LA1401 Thorlabs; L3: LC1611 Thorlabs; L4: LA1979 Thorlabs

from the edge of the incident beam on the sample to the edge of the integrating sphere port should be as large as practicable. This is to prevent light loss from the lateral sides of the sample. It has been demonstrated that when h is larger than five times of $1/(\mu_a + \mu'_s)$ the light loss from the lateral sides could be negligible. In order to perform transmittance and reflectance measurements on specimen that is only available in small size (smaller than the original spectrophotometer port size and the beam size on both ports), we designed and developed a small sample kit to adapt the original spectrophotometer setup. The small sample kit included 1) an adjustable slit to reduce the beam dimension at the beam exit port in the primary sample chamber (shown in Figure 1 (C)); 2) lenses sets to focus the incident beam at the transmittance and reflectance ports, respectively; 3) sample holder to hold the sample slide and to create a mask on the original port with reduced port size (shown in Figure 1 (B, D)). It is worth noting that the side facing the integrating sphere of the small sample holder consists of a patch of polytetrafluoroethylene (PTFE) sheet (99% reflectance, Zenith Lite, Pro-Lite Technology, UK) that covers the original port on the integrating sphere. In the centre of the PTFE sheet is a square port defining new sample port size. The PTFE material matches the material of the integrating sphere inner wall material Spectralon®. We developed two sets of the small sample kit with configurations listed in Table 1.

2.3. Two-tier Inverse Adding Doubling

To derive optical absorption and reduced scattering spectra from transmittance and reflectance spectra, we developed a two-tier IAD algorithm based on the open source IAD algorithm developed by [16] <https://github.com/scottprahl/iad>. In general, inverse adding doubling is a numerical approach to solve the radiative transport equation (RTE) providing analytical calculation of the optical properties of a sample slab from reflectance and transmittance measurements. The algorithm first assumes a thin slab with known optical properties and calculates the transmittance and reflectance at the slab surface, doubles them as adding another thin layer slab of the same material iteratively until the measured values of transmittance and reflectance are matched with those corresponding to the estimated optical properties. The algorithm can be conveniently used with integrating sphere measurements where the geometrical parameters such as port size of an integrating sphere, number of measurements, dimensions of the sphere, size of the incident light beam and the refractive index of the given biological sample have been

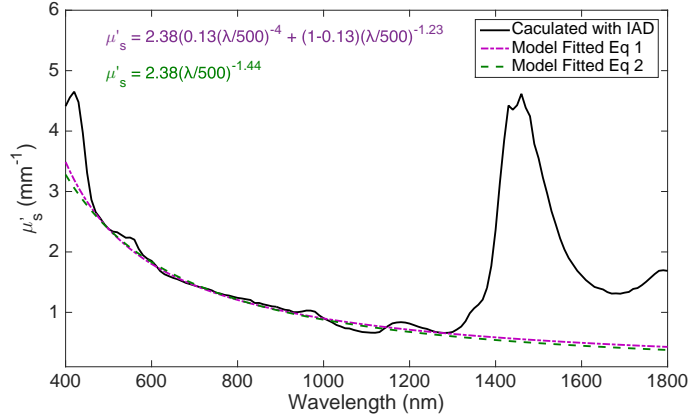


Figure 2. A representative sample of reduced scattering that was calculated from the measured total transmittance and total reflectance using the IAD algorithm. There are noticeable discrepancies at 420 nm, 560 nm and 1450 nm, between the calculated μ'_s and the ones fitted by Mie theory.

considered and accounted in the algorithm. However, a propound cross talk effect in the IAD calculated reduced scattering at the wavelength regions where the sample's absorption is much high (e.g. at 420 nm where haemoglobin absorption peak is, and at 1450 nm where the predominate water absorption peak is) was observed in our tissue experiments (shown in Figure 2, [25, 26]) and as well as reported and investigated in the work by *Gebhart et al.* [27]. To mitigate the inter-parameter cross talk effect, we proposed a two-tier inverse adding doubling process as shown in Figure 3. In the **first tier IAD**, we calculated an intermediate μ_a^{iad} and μ_s^{iad} . We fitted the μ_s^{iad} with power law according to the Mie theory,

$$\mu_s^{iad+fitted} = a_0 \left(\frac{\lambda}{\lambda_{ref}} \right)^{b_{Mie}} \quad (1)$$

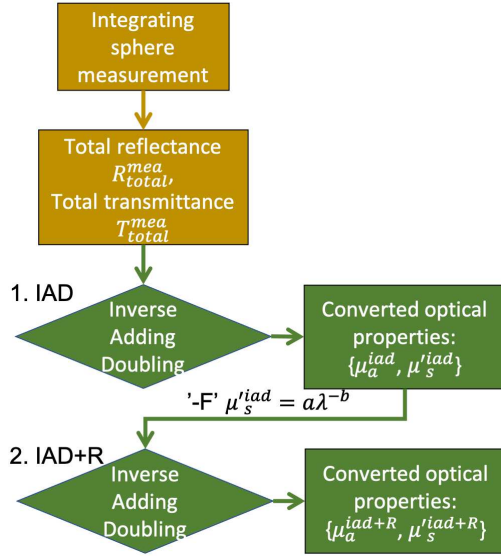
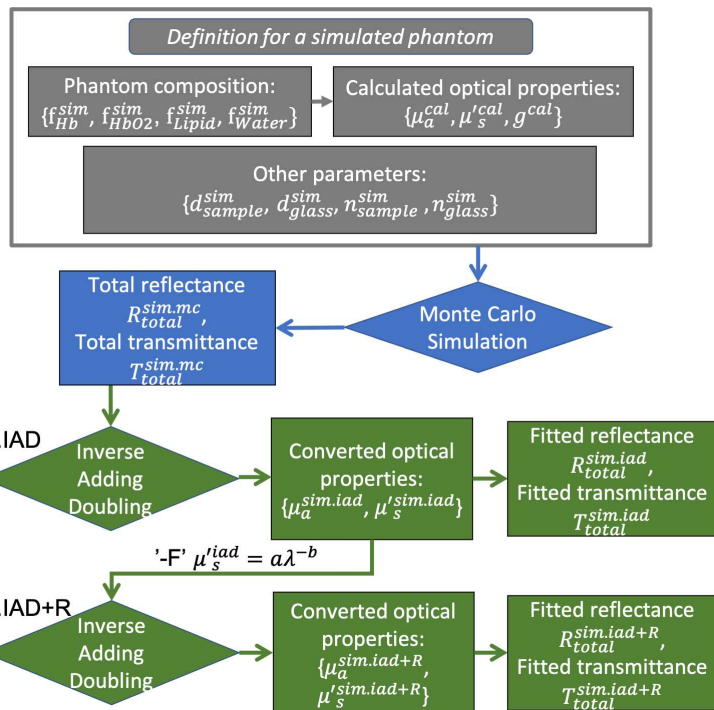
where a_0 is μ_s^{iad} value at 500 nm, and λ_{ref} is 500 nm. Then, we utilised the command line option '-F' for the **second tier IAD**.

By doing so, we reinforced the IAD to take the μ_s^{iad} to constrain the reduced scattering coefficient when computing. The final output of absorption and reduced scattering were denoted as μ_a^{iad+R} and μ_s^{iad+R} , respectively.

2.4. Validation of two-tier IAD with simulated data

$$\mu_a^{sim}(\lambda) = [\mu_a^{Hb}(\lambda) \ \mu_a^{HbO2}(\lambda) \ \mu_a^{Water}(\lambda) \ \mu_a^{Lipid}(\lambda)] \begin{bmatrix} f_{Hb}^{sim} \\ f_{HbO2}^{sim} \\ f_{Water}^{sim} \\ f_{Lipid}^{sim} \end{bmatrix} \quad (2)$$

To validate the proposed two-tier IAD, we first used computer-synthetic phantoms and their transmittance and reflectance spectra which were simulated by Monte

**Figure 3.** The work flow of the two-tier IAD algorithm.**Figure 4.** A flowchart diagram to illustrate the work flow of the validation process with computer simulated data.

Carlo modeling of light transport in Multi-Layered tissues (MCML) algorithm (<https://omlc.org/software/mc/>) [28, 29]. The work flow of the procedure includes the following steps:

- (i) Define a synthetic phantom consisting of four chromophores (Hb, HbO_2 , Water, Lipid) that are main constituents in most biological tissues. Assign each of them a volume fraction $f_{\text{Hb}}^{\text{sim}}$, $f_{\text{HbO}_2}^{\text{sim}}$, $f_{\text{Water}}^{\text{sim}}$, $f_{\text{Lipid}}^{\text{sim}}$.
- (ii) Calculate the total absorption spectrum μ_a^{cal} of the phantom based on the known respective absorption spectra of the four chromophores μ_a^{Hb} , $\mu_a^{\text{HbO}_2}$, μ_a^{Water} , μ_a^{Lipid} in its pure form and their volume fractions (Eq.2) [19, 30]; Reduced scattering μ_s^{cal} and anisotropy coefficient g^{cal} is calculated with the formula (Eq.4) presented in Aernouts *et al.* (2014) work [31].
- (iii) Define the phantom's thickness d , and refractive index n to be the inputs for Monte Carlo Simulation to generate total reflectance $R_{\text{total}}^{\text{sim,mc}}$ and total transmittance $T_{\text{total}}^{\text{sim,mc}}$ spectra of the phantom.
- (iv) Use IAD to calculate absorption $\mu_a^{\text{sim,iad}}$ and reduced scattering $\mu_s^{\text{sim,iad}}$ of the phantom from the $R_{\text{total}}^{\text{sim,mc}}$ and $T_{\text{total}}^{\text{sim,mc}}$.
- (v) Fit $\mu_s^{\text{sim,iad}}$ with simple power-law according to the Mie theory.
- (vi) In the second tier IAD, we used the fitted reduced scattering $\mu_s^{\text{sim,iad+fitted}}$ as input constrain of IAD to calculate a revised $\mu_a^{\text{iad+R}}$, and repeated step 4 to get the revised absorption coefficient $\mu_a^{\text{sim,iad+R}}$.
- (vii) Compare absorption and reduced scattering derived from the two-tier IAD ($\mu_a^{\text{sim,iad+R}}$, $\mu_s^{\text{sim,iad+fitted}}$) with the ones from original IAD ($\mu_a^{\text{sim,iad}}$, $\mu_s^{\text{sim,iad}}$) and the simulated ones ($\mu_a^{\text{sim,iad}}$, $\mu_s^{\text{sim,iad}}$) as validation.

2.5. Validation of two-tier IAD and small sample kit with integrating sphere measurement

We also performed validation on standard physical phantoms of which the absorption coefficient and reduced scattering coefficient can be precisely calculated from the phantoms' compositions. The procedure was similar to the one for validation on simulated data, except we used the spectrophotometer to measure the total transmittance and total reflectance of the physical phantom (work flow shown in Figure.5).

Phantom preparation: Liquid phantoms using lipid emulsion (Intralipid[®] 20%, Fresenius Kabi, UK) as scattering agent and hemoglobin (lyophilized powder, H2500 Sigma-Aldrich) as absorber. Intralipid has been demonstrated as a reliable material for introducing controllable scattering property in phantoms of which the optical properties and stability has also been fully investigated and reported ([32, 33, 31, 34, 35, 36, 37]). The batch-to-batch variations of the reduced scattering coefficient of Intralipid were found to be about 2%, while its absorption coefficient in the visible wavelength range is negligible and practically equal to absorption of water. Likewise, hemoglobin solution

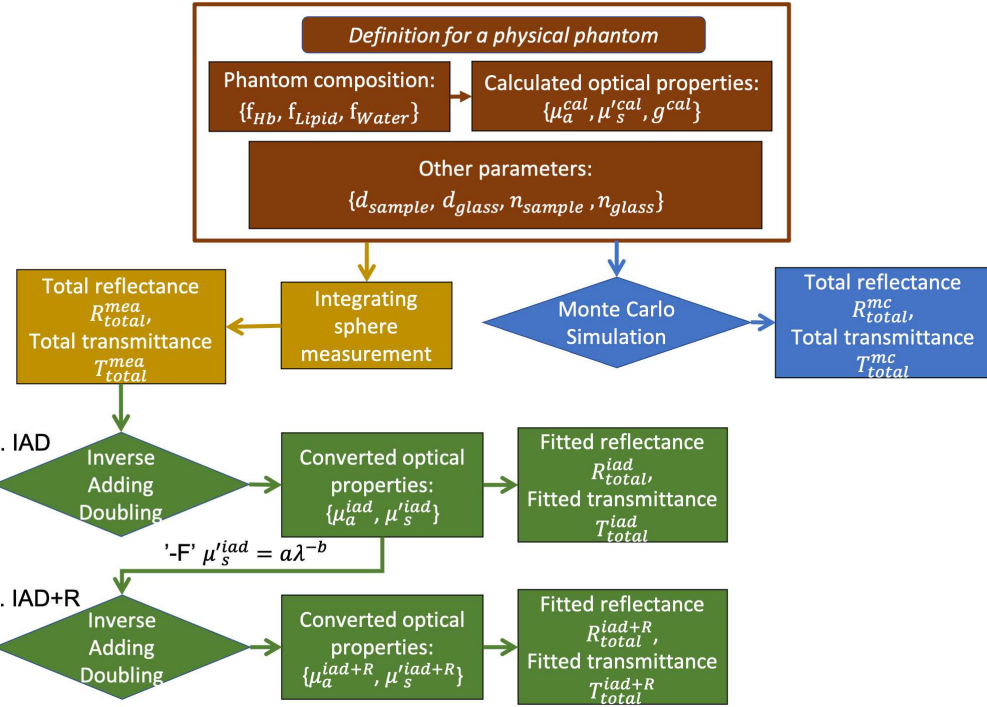


Figure 5. A flowchart diagram to illustrate the work flow of the validation process with integrating sphere measurements.

has been widely used in optical phantom preparation and its extinction coefficient is available from literature [38, 39, 40, 41]. It should be noted, since native hemoglobin is readily oxidized in air during the supplier's manufacture process, the lyophilized powder of hemoglobin may be predominantly methemoglobin (MetHb) of which the extinction coefficient is different to the Hb and HbO [42, 43]. We then used the spectrophotometer to measure the absorption coefficient of the methemoglobin/hemoglobin solution prepared from lyophilized powder of bovine hemoglobin 1.0 mg/ml. We also calculated the absorption coefficient of 10% Intralipid as reported in the work of *Michels et al.*, (2008) [32]. In summary, the absorption coefficient spectra of the substances (μ_a^{IL10} , μ_a^{MetHb} , μ_a^{Water}) we used for the phantom preparation are shown in Figure 6. The phantom consisted of 1.25 mg/ml bovine hemoglobin and 7.5% Intralipid, and was prepared with water at room temperature (ca. 21°C). The absorption and scattering coefficient of the liquid phantom were calculated with below formulas:

$$\mu_a = \begin{cases} \mu_a^{MetHb} \times 1.25 + \mu_a^{IL10} \times 0.75 & 400 \text{ nm} \leq \lambda < 1400 \text{ nm} \\ \mu_a^{Water} & 1400 \text{ nm} \leq \lambda \leq 1800 \text{ nm} \end{cases} \quad (3)$$

$$\mu_s(\lambda) = \frac{1.868e-10 \lambda^{-2.59}}{0.227} \Phi_{lip} \frac{(1 - \Phi_{lip})^{p(\lambda)+1}}{(1 + \Phi_{lip}(p(\lambda) - 1))^{p(\lambda)-1}}$$

$$p(\lambda) = 1.31 + 0.0005481\lambda$$

$$g(\lambda) = 1.1 - (0.58e-3\lambda)$$

$$\mu'_s(\lambda) = \mu_s(\lambda)g(\lambda)$$

$$(4)$$

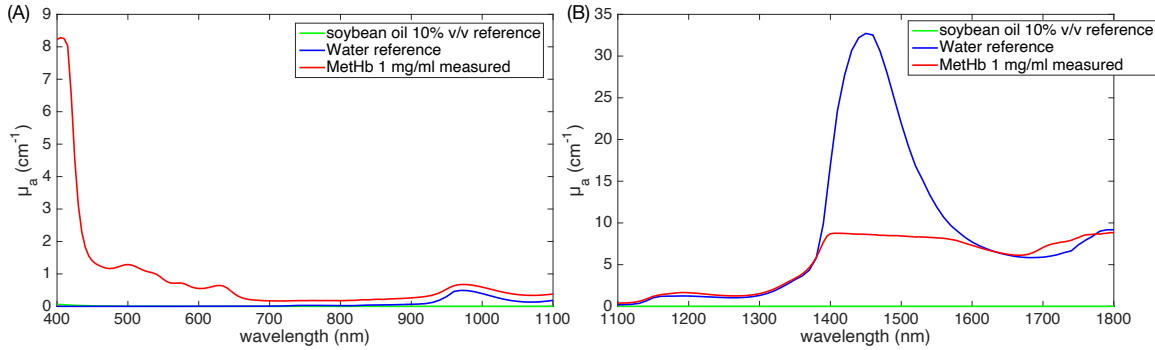


Figure 6. Absorption coefficient spectra of 1 mg/ml methemoglobin as measured by spectrophotometer, and 10% Intralipid as calculated from [32], and water as from reference.

where Φ_{lip} is the volume concentration of Intralipid which is 0.075. The refractive index of the phantom was calculated based on the volume concentration of scattering particles or lipid (Φ_{lip}) in the phantom $n_{phantom} = n_{water} + 0.14\Phi_{lip}$ [44]. We also designed and developed sample chambers to contain liquid phantom samples for integrating sphere measurements. The sample chamber consisted of two glass slides 52 mm (w) x 76 mm (h) x 1 mm (d), and a 2 mm thick U shape acrylic spacer that was processed by a laser cutter (VLS6.75, Universal Laser Systems, USA) and glued between the two glass slides with a UV-curing optical adhesive (NOA68, Thorlabs, USA).

Small sample kit: To validate the measurement with small sample kit, we used the liquid phantom developed as described in the previous section 2.5 and measured in the spectrophotometer with the 3 mm sample kit and 5 mm sample kit.

3. Results & Discussions

The computer simulated phantom comprised oxy- and deoxy- haemoglobin (HbO_2 , Hb), water and lipid with given volume fractions as displayed in Figure 7 (C). Results of absorption coefficient spectra and reduced scattering spectra ($\mu_a^{sim.iad+R}, \mu_s^{sim.iad+R}$) of the phantom using the proposed two-tier IAD process are presented in Figure 7. The values are compared to results by original IAD algorithm ($\mu_a^{sim.iad}, \mu_s^{sim.iad}$) and as well as the calculated ground truth values (μ_a^{sim}, μ_s^{sim}). There is a noticeable discrepancy between the IAD derived $\mu_a^{sim.iad}$ and the calculated ground truth μ_a^{sim} at $\lambda = 420 \text{ nm}$ which is affected by the cross talk with $\mu_s^{sim.iad}$ as shown in Figure 7 (C, D). The underestimated absorption is successfully corrected by applying the second layer of IAD as proposed. The corrected $\mu_a^{sim.iad+R}$ aligns greatly with the ground truth μ_a^{sim} (Figure 7 (C, D)). However, we noticed that on the longer wavelength region when $\lambda \geq 1400 \text{ nm}$ there is noticeable discrepancy between the resulting values and the ground truth. This is presumably caused by using the simple power law fitted μ_s^{iad} as the constrain for the second layer of IAD computing, the residuals of the fitting model are higher at the longer wavelength range. More detailed modelling such as including Rayleigh scattering could

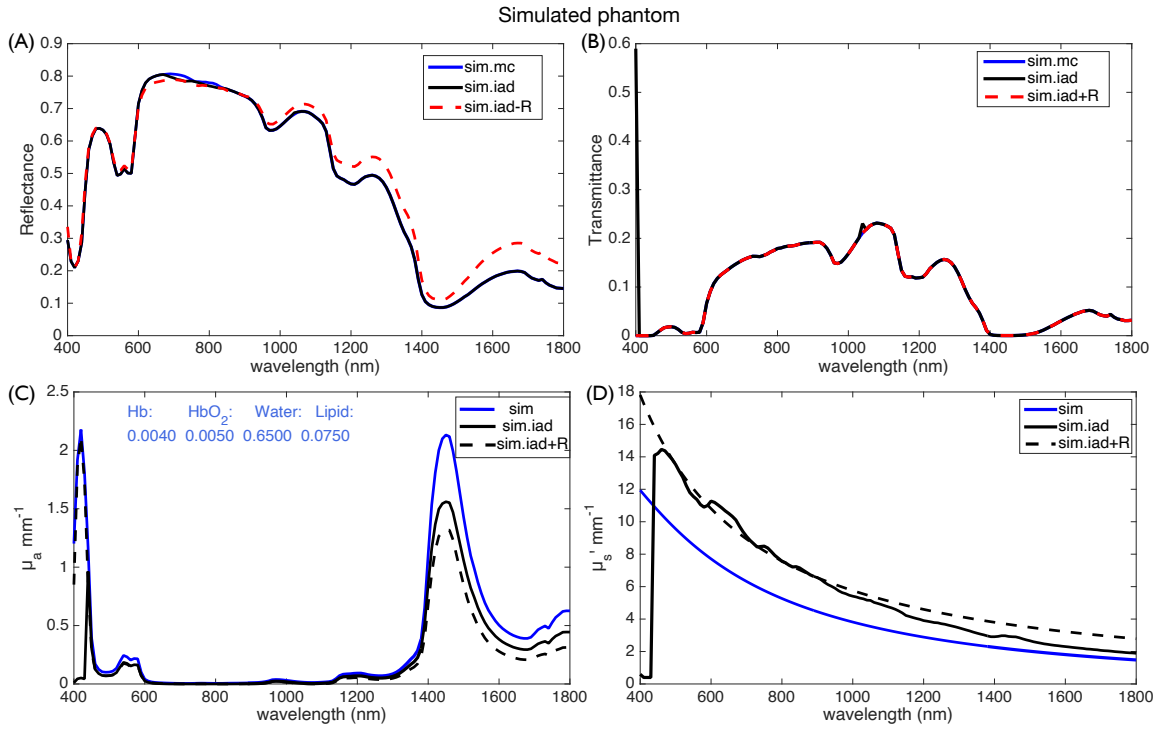


Figure 7. Data of a computer simulated phantom which comprises oxy- and deoxy-haemoglobin (HbO_2 , Hb), water and lipid with given volume fractions. A-B: Total reflectance and total transmittance spectra of the synthetic phantom A, generated by Monte Carlo simulation, and IAD respectively. C-D: Absorption and reduced scattering spectra of phantom A that are calculated with the two-tier IAD respectively. It is worth noting that in the longer wavelength range ($\lambda > 1400 \text{ nm}$) the proposed two-tier IAD method deteriorated the reconstruction of absorption spectrum μ_a^{iad+R} (C). Presumably, this was because the simple power law fitting with input constraints used in the second tier IAD calculation was not capable of accurately modelling the reduced scattering spectrum over a broad range of wavelength (D).

mitigate the discrepancies and will be further investigated. Simulated transmittance spectra and reflectance spectra by using MCML algorithm and the values were derived with IAD algorithms are also presented in Figure 7 (A, B). As a result of two-tier IAD the pronounced discrepancy of the transmittance spectra at $\lambda = 420 \text{ nm}$ was rectified. We also notice that $\mu_a^{sim.iad+R}$, $\mu_s^{sim.iad+R}$ mostly changed the reflectance spectra rather than transmission spectra.

The liquid phantom was produced and measured in the integrating sphere with the standard set-up first. The phantom sample dimension was 40 mm (w) x 50 mm (h) x 2 mm (d) which was defined by the size of the sample chamber. The absorption coefficient spectra and reduced scattering spectra (μ_a^{iad+R} , μ_s^{iad+R}) of the liquid phantom using the two-tier IAD process are presented in Figure 8. For absorption coefficient, the values are compared to results by original IAD algorithm (μ_a^{iad}) and as well as the calculated ground truth values (μ_a^{cal} , μ_s^{cal}), showing a good agreement across the whole wavelength range. There is an offset between the μ_s^{iad+R} and the calculated ground truth values (μ_s^{cal}).

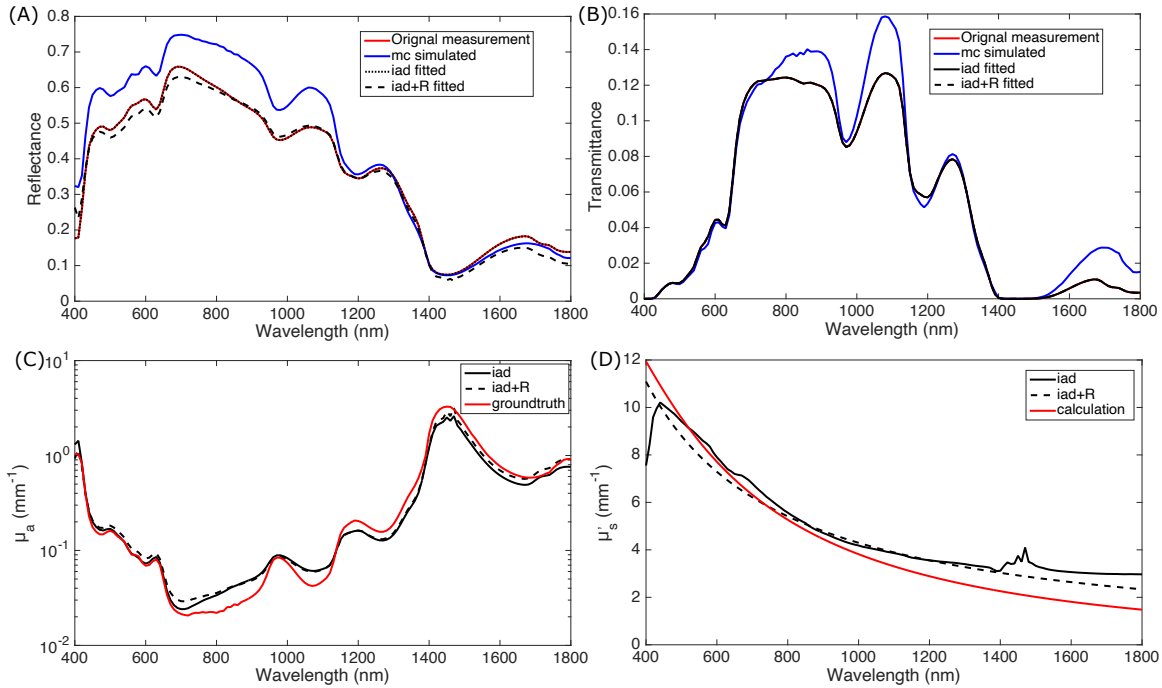


Figure 8. Results of validation process for the proposed two-tier IAD algorithm.

We also compared the transmittance spectra and reflectance spectra calculated by using the IAD algorithm to the values from integrating sphere measurements and simulated values by using MCML algorithm (Figure 8 (A, B)). The liquid phantom sample from the same freshly-prepared batch were then measured with small sample kits. The phantom sample dimension was 7 mm (w) x 15 mm (h) x 2 mm (d) defined by the size of the sample chamber. The distance As as expected, the reflectance and transmittance spectra measured with small sample kits were lower than the ones with original set-ups, which were attributed to the light loss on the lateral sides of the sample. The distance (h_t) from the edge of the incident beam on the sample to the edge of the adapted integrating sphere transmittance ports were calculated as 1 mm for the 3 mm port and 1.5 mm for the 5 mm port. h_r for the reflectance ports were calculated as 0.5 mm and 0.75 mm for the 3 mm port and 5 mm port, respectively. For the liquid phantom sample we used here, the $1/(\mu_a + \mu'_s)$ value is greater than $1/8$ roughly at $\lambda = 430 - 1400$ nm. Consequently, the h value is less than five times of $1/(\mu_a + \mu'_s)$ resulting in noticeable light loss. Further study direction will be on the investigation of the influence of sample optical properties on the accuracy of using small port size and condensed beam.

In Figure 10, the absorption coefficient and the reduced scattering coefficient spectra are presented for different anisotropy factors ranging from 0.45 to 0.95. The absorption coefficient and the reduced scattering coefficient were not changed significantly by changing the anisotropy factor.

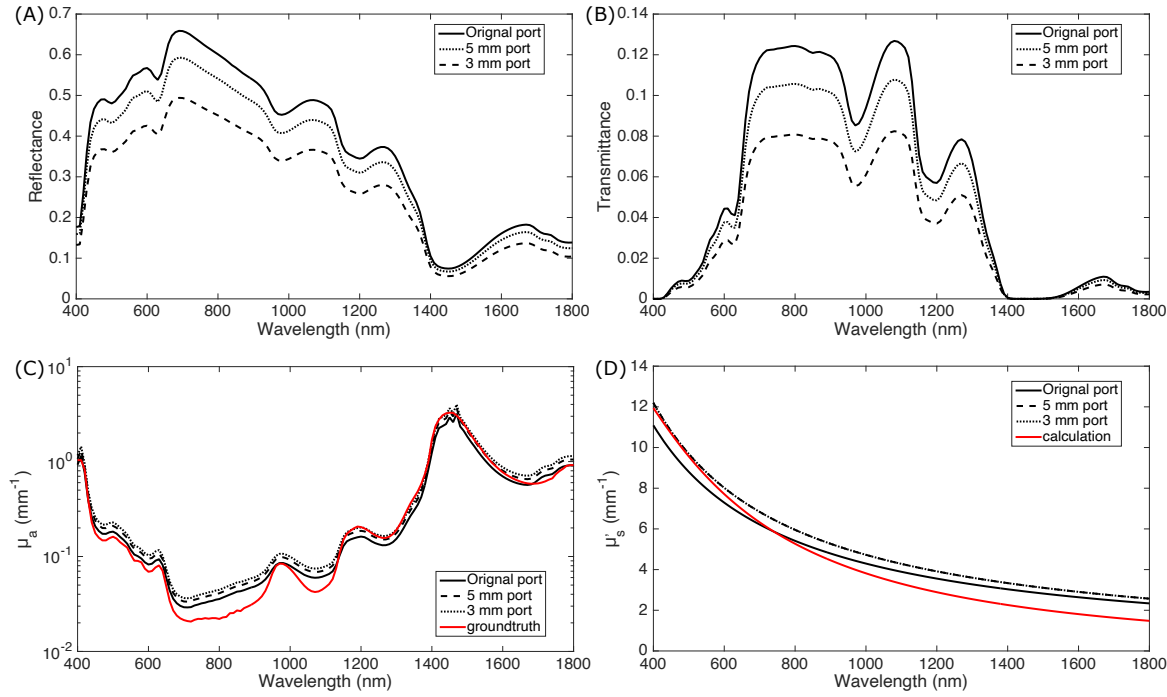


Figure 9. Spectrophotometer integrating sphere measurements (A, B) of small samples of liquid phantom using the small sample kit and the converted optical properties using the two-tier IAD as validated against the original sample port. Optical absorption coefficients (C) and Reduced scattering (D) of liquid phantom using different port sizes.

4. Conclusions

Our work suggests that the proposed two-tier IAD process will generate a revised absorption spectrum using the fitted reduced scattering of which the cross talk effect is mitigated as an input constrain. And the revised absorption spectrum is evaluated in the phantom simulation study to be accurate to the ground truth, especially in the wavelength range where the cross talk is evident. The proposed small sample kits were validated against standard integrating sphere spectrophotometer measurements on a well-characterised liquid phantom. Our proposed method of a two-tier IAD and small sample kit could be a useful and reliable tool to characterise optical properties of biological tissue *ex vivo* particularly when only small size samples are available.

Acknowledgments

This work was supported by the Wellcome Trust [203145Z/16/Z; 203148/Z/16/Z; WT106882], EPSRC [NS/A000050/1; NS/A000049/1], and by core funding from the Wellcome/EPSRC Centre for Medical Engineering [WT203148/Z/16/Z]. YX is supported by the L'Oréal-UNESCO UK and Ireland For Women in Science Rising Talent Programme. TV is supported by a Medtronic / Royal Academy of Engineering Research Chair [RCSR1819/7/34].

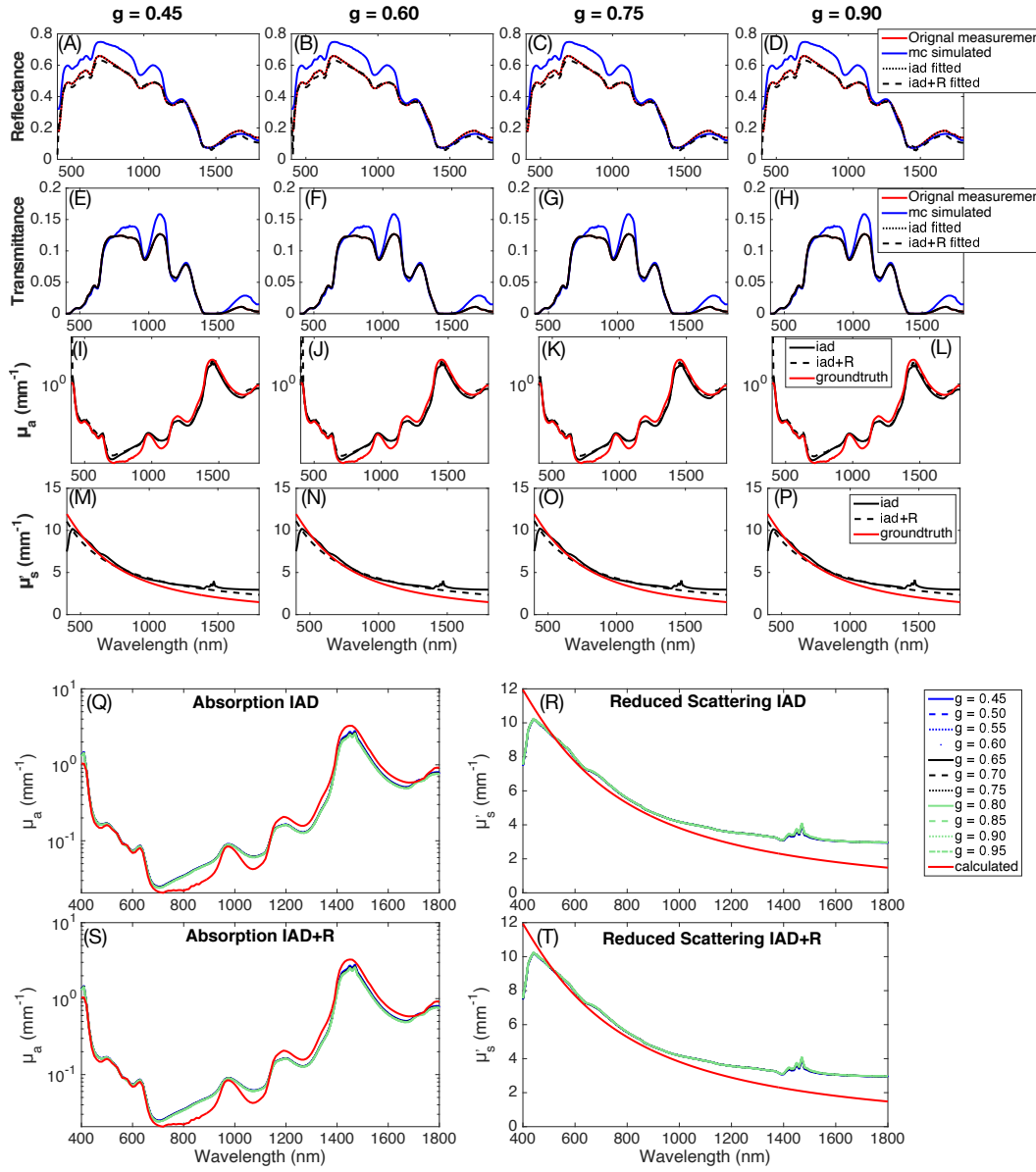


Figure 10. Absorption coefficient spectra and reduced scattering coefficient spectra of phantom, when the anisotropy factor g was altered from 0.45 - 0.95.

5. Reference

- [1] Xie Y, Bonin T, Loeffler S, Huettmann G, Tronnier V and Hofmann U G 2010 Fiber spectral domain optical coherence tomography for in vivo rat brain imaging *Biophotonics: Photonic Solutions for Better Health Care II*. ed Popp J, Drexler W, Tuchin V V and Matthews D L (SPIE) pp 77152F-77152F-9
- [2] Ebner M, Nabavi E, Shapey J, Xie Y, Liebmann F, Spirig J M, Hoch A, Farshad M, Saeed S R, Bradford R, Yardley I, Ourselin S, Edwards A D, Führnstaedt P and Vercauteren T 2021 *Journal of Physics D: Applied Physics* **54** ISSN 13616463
- [3] Shapey J, Xie Y, Nabavi E, Bradford R, Saeed S R, Ourselin S and Vercauteren T 2019 *Journal of Biophotonics* **12** ISSN 18640648
- [4] Charalampaki P, Javed M, Daali S, Heiroth H J, Igressa A and Weber F 2015 *Neurosurgery* **62 Suppl 1** 171–176 ISSN 1524-4040 URL <http://www.ncbi.nlm.nih.gov/pubmed/26181939>
- [5] Stummer W, Tonn J C, Goetz C, Ullrich W, Stepp H, Bink A, Pietsch T and Pichlmeier U 2014 *Neurosurgery* **74** 310–319 ISSN 0148396X
- [6] Zharkikh E, Dremin V, Zherebtsov E, Dunaev A and Meglinski I 2020 *Journal of Biophotonics* **13** 1–20 ISSN 18640648
- [7] You J, Pan C, Park K, Li A and Du C 2020 *Journal of Biophotonics* **13** 1–11 ISSN 18640648
- [8] Heijblom M, Piras D, Xia W, van Hespen J, Klaase J, van den Engh F, van Leeuwen T, Steenbergen W and Manohar S 2012 *Optics Express* **20** 11582 ISSN 1094-4087
- [9] Magnain C, Augustinack J C, Konukoglu E, Frosch M P, Sakadžić S, Varjabedian A, Garcia N, Wedeen V J, Boas D a and Fischl B 2015 *Neurophotonics* **2** 015004 ISSN 2329-423X
- [10] Escobar P F, Rojas-Espaillet L, Tisci S, Enerson C, Brainard J, Smith J, Tresser N J, Feldchtein F I, Rojas L B and Belinson J L 2006 *International journal of gynecological cancer : official journal of the International Gynecological Cancer Society* **16** 1815–22 ISSN 1048-891X URL <http://www.ncbi.nlm.nih.gov/pubmed/17009977>
- [11] Desroches J, Jermyn M, Pinto M, Picot F, Tremblay M A, Obaid S, Marple E, Urmey K, Trudel D, Soulez G, Guiot M C, Wilson B C, Petrecca K and Leblond F 2018 *Scientific Reports* **8** 1–10 ISSN 20452322
- [12] Jermyn M, Mok K, Mercier J, Desroches J, Pichette J, Saint-Arnaud K, Bernstein L, Guiot M C, Petrecca K and Leblond F 2015 *Science Translational Medicine* **7** 19–274 ISSN 1946-6234 URL <https://stm.sciencemag.org/lookup/doi/10.1126/scitranslmed.aaa2384>
- [13] Campagnola P 2011 *Analytical Chemistry* **83** 3224–3231 ISSN 0003-2700
- [14] Sibai M, Wirth D J, Leblond F, Roberts D W, Paulsen K D and Wilson B C 2019 *Journal of Biophotonics* 1–6 ISSN 18640648
- [15] Sun Y, Hatami N, Yee M, Phipps J, Elson D S, Gorin F, Schrot R J and Marcu L 2010 *Journal of biomedical optics* **15** 056022 ISSN 1560-2281 URL <http://www.ncbi.nlm.nih.gov/pubmed/21054116> http://www.ncbi.nlm.nih.gov/entrez/query.fcgi?cmd=Retrieve&db=PubMed&list_uids=21054116&dopt=Abstract
- [16] Prahl S A, van Gemert M J C and Welch A J 1993 *Applied Optics* **32** 559 ISSN 0003-6935
- [17] Rejmstad P, Zsigmond P and Wårdell K 2017 *Optics Express* **25** 8192 ISSN 1094-4087
- [18] Crane N J, Huffman S W, Gage F A, Levin I W and Elster E A 2003 *Journal of Biomedical Optics* **18** 035001–7
- [19] Nachabé R, Hendriks B H W, van der Voort M, Desjardins A E and Sterenborg H J C M 2010 *Biomedical Optics Express* **1** 1432 ISSN 2156-7085
- [20] Wisotzky E L, Uecker F C, Dommerich S, Hilsmann A, Eisert P and Arens P 2019 *Journal of Biomedical Optics* **24** 1 ISSN 1560-2281
- [21] Mesradi M, Genoux A, Cuplov V, Haidar D A, Jan S, Buvat I, Pain F, Mesradi M, Genoux A, Cuplov V, Haidar D A, Jan S and Pain F 2013 *Journal of biomedical optics* **18** 117010
- [22] Jernshøj K D and Hassing S 2009 *Applied Spectroscopy* **63** 879–888 ISSN 00037028
- [23] Gaigalas A K, Wang L and Choquette S 2013 *Journal of Research of the National Institute of Standards and Technology* **118** 1–10 ISSN 2470-3307

Standards and Technology **118** 1–14 ISSN 21657254

- [24] Rehman A u, Ahmad I and Qureshi S A 2020 *Photodiagnosis and Photodynamic Therapy* **31** ISSN 18731597
- [25] Shapey J, Xie Y, Nabavi E, Ebner M, Maneas E, Saeed S R, Dorward N, Kitchen N, Desjardins A E, Ourselin S, Jaunmuktane Z, Brandner S, Bradford R and Vercauteren T 2020 *Spie*
- [26] Shapey J, Xie Y, Nabavi E, Ebner M, Saeed S R, Kitchen N, Dorward N, Grieve J, McEvoy A W, Misericocchi A, Grover P, Bradford R, Lim Y M, Ourselin S, Brandner S, Jaunmuktane Z and Vercauteren T 2021 *Journal of Biophotonics* **Under review**
- [27] Gebhart S C, Lin W C and Mahadevan-Jansen A 2006 *Physics in Medicine and Biology* **51** 2011–2027 ISSN 00319155
- [28] L Wang, S L Jaques and L Zheng 1995 *Computer Methods and Programs in Biomedicine* **47** 131–146
- [29] Wang L, Jacques S L and Zheng L 1997 *Computer Methods and Programs in Biomedicine* **54** 141–150 ISSN 01692607 URL <https://linkinghub.elsevier.com/retrieve/pii/S0169260797000217>
- [30] Nachabé R, Hendriks B H W, Desjardins A E, van der Voort M, van der Mark M B and Sterenborg H J C M 2010 *Journal of Biomedical Optics* **15** 037015 ISSN 10833668
- [31] Aernouts B, Van Beers R, Watté R, Lammertyn J and Saeys W 2014 *Optics Express* **22** 6086 ISSN 1094-4087
- [32] Michels R, Foschum F and Kienle A 2008 *Optics Express* **16** 5907 ISSN 1094-4087 URL <https://www.osapublishing.org/oe/abstract.cfm?uri=oe-16-8-5907>
- [33] Di Ninni P, Bérubé-Lauzière Y, Mercatelli L, Sani E and Martelli F 2012 *Applied Optics* **51** 7176 ISSN 1559-128X
- [34] Spinelli L, Botwicz M, Zolek N, Kacprzak M, Milej D, Sawosz P, Liebert A, Weigel U, Durduran T, Foschum F, Kienle A, Baribeau F, Leclair S, Bouchard J P, Noiseux I, Gallant P, Mermut O, Farina A, Pifferi A, Torricelli A, Cubeddu R, Ho H C, Mazurenka M, Wabnitz H, Klauenberg K, Bodnar O, Elster C, Bénazech-Lavoué M, Bérubé-Lauzière Y, Lesage F, Khoptyar D, Subash A A, Andersson-Engels S, Di Ninni P, Martelli F and Zaccanti G 2014 *Biomedical Optics Express* **5** 2037 ISSN 2156-7085
- [35] Krauter P, Nothelfer S, Bodenschatz N, Simon E, Stocker S, Foschum F and Kienle A 2015 *Journal of Biomedical Optics* **20** 105008 ISSN 1083-3668
- [36] Samkoe K S, Bates B D, Tselepidakis N N, DSouza A V and Gunn J R 2017 *Journal of Biomedical Optics* **22** 1 ISSN 1560-2281
- [37] Fredriksson I, Saager R B, Durkin A J and Strömberg T 2017 *Journal of Biomedical Optics* **22** 1 ISSN 1560-2281
- [38] Pogue B W and Patterson M S 2006 *Journal of Biomedical Optics* **11** 041102 ISSN 10833668
- [39] Lamouche G, Kennedy B F, Kennedy K M, Bisailon C E, Curatolo A, Campbell G, Pazos V and Sampson D D 2012 *Biomedical Optics Express* **3** 1381 ISSN 2156-7085
- [40] Haj-Hosseini N, Kistler B and Wårdell K 2014 *Proceedings of SPIE* **8945** 1–6 ISSN 16057422 URL <http://proceedings.spiedigitallibrary.org/proceeding.aspx?doi=10.1117/12.2039861>
- [41] Du Le V N, Nie Z, Hayward J E, Farrell T J and Fang Q 2014 *Biomedical Optics Express* **5** 2726 ISSN 2156-7085 URL <https://www.osapublishing.org/boe/abstract.cfm?uri=boe-5-8-2726>
- [42] Cruz-Landeira A, Bal M J, Quintela O and López-Rivadulla M 2002 *Journal of Analytical Toxicology* **26** 67–72 ISSN 01464760
- [43] Zijlstra W G and Buursma A 1997 *Comparative Biochemistry and Physiology - B Biochemistry and Molecular Biology* **118** 743–749 ISSN 03050491
- [44] Aernouts B, Zamora-Rojas E, Van Beers R, Watté R, Wang L, Tsuta M, Lammertyn J and Saeys W 2013 *Optics Express* **21** 32450 ISSN 1094-4087